

Constructing regular black holes from multi-polytropic equations of state

Seyed Naseh Sajadi,^{1,*} Supakchai Ponglertsakul,^{1,†} and Orlando Luongo^{2,3,4,5,6,‡}

¹*Strong Gravity Group, Department of Physics, Faculty of Science,
Silpakorn University, Nakhon Pathom 73000, Thailand.*

²*University of Camerino, Via Madonna delle Carceri, Camerino, 62032, Italy.*

³*SUNY Polytechnic Institute, 13502 Utica, New York, USA.*

⁴*INAF - Osservatorio Astronomico di Brera, Milano, Italy.*

⁵*Istituto Nazionale di Fisica Nucleare (INFN), Sezione di Perugia, Perugia, 06123, Italy.*

⁶*Al-Farabi Kazakh National University, Al-Farabi av. 71, 050040 Almaty, Kazakhstan.*

(Dated: February 5, 2025)

Regular black holes are imagined as solutions to Einstein's field equations, with no singularities, albeit characterized by the presence of an internal structure. With the intention not to use non-linear electrodynamics, we here propose to obtain new classes of solutions that can also satisfy the Tolman-Oppenheimer-Volkoff (TOV) equations, plus adding a non-zero core. Thus, we present regular black holes as solutions to the TOV equations using multipolytropic equations of state and investigate whether these solutions behave, tuning the underlying free parameters. Our analysis demonstrates that, within specific parameter ranges, repulsive gravity effects may occur in precise regions. Accordingly, black hole remnants are also investigated, showing that, under certain circumstances, they may turn into dark energy sources in view of the corresponding repulsive gravity effects, located outside the horizons. Moreover, quite remarkably, critical sets of parameters imply that solutions may exhibit transitions to regular repulsive relativistic compact objects from black hole behaviors. Finally, we explore the interpretation of these regular black hole solutions in terms of topological thermodynamic defects.

I. INTRODUCTION

Even though general relativity (GR) has successfully passed numerous experimental tests, theoretical inconsistencies seem to jeopardize Einstein's field equations at both infrared and ultraviolet regimes. For example, in the presence of strong gravitational fields, the lack of a complete quantum gravity theory [1, 2] and the issue of singularities are clearly unresolved challenges. Similarly, at cosmological scales, open questions remain toward cosmological tensions [3] and the nature of the universe's dark components [4–7].

Accordingly, the Penrose theorems state that gravitational collapse inevitably leads to curvature singularities [8] which GR fails to be predictive. Nevertheless, singularities are generally associated with phase transition and not common in nature with a notable exception of the Big Bang [9]. Consequently, the *singularity problem* is closely tied to the existence of black holes (BHs), whose reality has been strongly supported by the direct detection of gravitational waves and BH shadows [10, 11].

In view of a quantum gravity theory and of the fact that singularities are not physical frameworks, fully understanding BH properties may be required to avoid singularities or modify the corresponding classical theory, including quantum effects¹. Remarkably, singularities can be avoided if the energy conditions, assumed by the

singularity theorems are violated at least in some space-time regions. Regular regions can replace singularities with some exotic form of matter that violates the strong energy condition. Following the pioneering contribution by Sakharov and Gliner [13, 14], the first idea suggesting that singularities could be avoided is based on including a de Sitter core². Following this recipe, a wide class of regular BH (RBH) solutions has been released in the literature, see e.g. [16–19].

In this respect, the first smooth RBH, based on this prescription, is first proposed by Bardeen [20]. For completeness, RBHs have natural horizons but no singularities, placed at the center, i.e., the solution tends to be a de Sitter core solution and, generally, to a Schwarzschild solution asymptotically. In addition, Ayon-Beato and Garca successfully interpreted the Bardeen BH in the framework of non-linear electrodynamics [21]. Later, many other RBHs have been obtained invoking the aforementioned nonlinear electrodynamics in GR [22–26] and modified gravities, i.e., 4D Einstein Gauss-Bonnet gravity [27], $f(R)$ gravity [28] and $f(R, T)$ gravity [29].

Significant progress has been made in the study of regular BH physics over the past decades. In particular, RBHs have been explored in the context of quantum gravity, with possible quantum origins linked to modifications of the uncertainty principle [30]. Additionally, RBHs have been derived from pure gravitational theories in higher-dimensional frameworks [31]. Various aspects

*Electronic address: naseh.sajadi@gmail.com

†Electronic address: supakchai.p@gmail.com

‡Electronic address: orlando.luongo@unicam.it

¹ For effective quantum BH pictures, see [12].

² More precisely, de Sitter cores may be associated with vacuum energy contributions that avoid the presence of singularities. For a generalization of de Sitter solutions see [15].

of their properties have been investigated, including thermodynamics [32, 33], inner-horizon instability [34, 35], and observational signatures such as their shadows [36–39]. Furthermore, studies have examined RBH quasinormal modes [40–42], superradiance effects [43], and the potential existence of primordial RBHs [44].

Quite remarkably, it has been shown that the matter content of an RBH can exhibit a polytropic equation of state [45]. Almost all polytropic models assume an isotropic pressure, i.e., the tangential and radial components are the same. Recently, RBH is obtained by considering Kiselev black hole [46] surrounding by anisotropic fluid [47].

In general, however, all principal pressures can have double-polytropic equations of state, so, several authors have investigated anisotropic models that provide different pressures for the tangential and radial components, see e.g. [48–51]. For example, although the radial pressure vanishes at the surface of a compact star, one could postulate a tangential pressure to exist. While the latter does not alter the spherical symmetry, it may create some streaming fluid motions [52, 53]. In this respect, the Reissner-Nordström solution is another relativistic solution that is based on the existence of anisotropic stress tensor. A charged BH is associated with negative radial pressure, while the tangential pressure remains positive [54]. This anisotropic pressure originates from the fact that the particle’s phase space distribution function depends on coordinates and velocities only through the constants of motion (energy and angular momentum). If the distribution function depends on the magnitude of the angular momentum, this will lead to an anisotropic pressure, even if the system is spherically symmetric.

Motivated by the fact that there are two different ways to construct RBH, i.e., by solving the field equations associated with a special source of matter, whereas the second is to write a desired RBH solution at first, then determining *a posteriori* the corresponding action of matters. Here, we obtain RBH solutions inspired by solving the relativistic version of the classical hydrostatic equilibrium equation inspired by the TOV spacetime [55, 56] with a multi-component polytropic equations of state, hereafter multi-polytropic equations of state.

Hence, we allow non-zero anisotropic contributions to the pressure by assuming different tangential and radial components in the energy-momentum tensor and consider different equations of state, emphasizing specific cases that can be of particular interest. Here, the important point is that the regularity of a BH comes from the tangential pressure of its constituent matter, especially from the nonlinear part of the tangential pressure. This means that the multi-polytropic anisotropic perfect fluid is a suitable source for RBHs.

Traditionally, the polytropic equation of state has been used to describe a completely degenerate gas in white dwarfs and a completely convective star. Moreover, different parts of astrophysical objects may obey polytropic behavior but with different polytropic indices. It is

therefore reasonable to assume that an equation of state which is a mixture of different polytropes (i.e. a multi-polytropic equation of state) can be a better fit to the real equation of state. A multi-polytropic equation of state that is softer at low densities and stiffer at high densities may be appropriate for describing a hybrid astrophysical object. Afterwards, a more general equation of state provides a better fit, thereby increasing the freedom to describe naturally occurring astronomical objects.

The paper is organized as follows. In Section II, we solve the generalized TOV equation with an anisotropic equation of state. In sections III and IV, we present two RBHs and study the physical properties of the solutions, and the last section V reflects the concluding remarks of our work.

II. THE ANISOTROPIC TOV EQUATION

We here start considering statically and spherically symmetric spacetime with coordinates (t, r, θ, ϕ) , describing gravitating relativistic object

$$ds^2 = -f(r)dt^2 + h(r)dr^2 + r^2d\theta^2 + r^2\sin^2\theta d\phi^2, \quad (1)$$

where $f(r)$ and $h(r)$ denote the unknown lapse and shift functions, respectively. From Einstein’s field equations, $\mathcal{R}_{\mu\nu} - \frac{1}{2}g_{\mu\nu}\mathcal{R} = 8\pi G\mathcal{T}_{\mu\nu}$, considering an anisotropic fluid, we write the energy-momentum tensor,

$$\mathcal{T}_{\nu}^{\mu} = \text{diag}(-\rho, P_r, P_t, P_t), \quad (2)$$

here ρ , P_r , and P_t are the energy density, radial and transverse components of the pressure, respectively.

Let’s introduce the mass variable $M(r)$ via

$$h(r) = \left(1 - \frac{2GM(r)}{r}\right)^{-1}, \quad (3)$$

where $M(r)$ is interpreted as the gravitational mass inside radius r , satisfying

$$M(r) = \int_0^r 4\pi\tilde{r}^2\rho(\tilde{r})d\tilde{r}, \quad (4)$$

that also relates the density, ρ , and the mass, M .

From the TOV spacetime and adopting $\nabla_{\mu}\mathcal{T}_{\nu}^{\mu} = 0$, we infer the equation for the radial and tangential pressures,

$$-P_r' = \frac{G(\rho + P_r)(M + 4\pi r^3 P_r)}{r(r - 2M)} + \frac{2(P_r - P_t)}{r}, \quad (5)$$

where prime denotes derivative with respect to r . Remarkably, the effect of anisotropy is evident within the last term of (5). To seek an RBH class of solution, we first assume the following barotropic equations of state (EoS) [57–59]

$$P_r = \omega\rho + \bar{\omega}\frac{\rho^n}{\rho_0^{n-1}}, \quad (6)$$

$$P_t = \omega_1\rho + \omega_2\frac{\rho^m}{\rho_0^{m-1}}, \quad (7)$$

here $\rho_0 > 0$ is the central density, $\omega, \bar{\omega}, \omega_1$ and ω_2 , are the dimensionless EoS parameters.

The first term, appearing in (6)–(7), is the widely-used linear EoS, where the sound speed contribution is constant, whereas the second term allows for a polytropic behavior, adopted to characterize stars and/or interiors, e.g. leading to the Lane-Emden equation in the theory of stellar structure. In addition, the polytropic EoS is also used in several cosmological realms, see e.g. [60].

To obtain the solutions with $\mathcal{T}_t^t = \mathcal{T}_r^r$ resulting into the Schwarzschild coordinates, namely $f = h^{-1}$, we require $\omega = -1, \bar{\omega} = 0$. Thus, the anisotropic fluid consists of the following components of the pressure:

$$P_r = -\rho, \quad P_t = \omega_1 \rho + \omega_2 \frac{\rho^m}{\rho_0^{m-1}}. \quad (8)$$

Plugging the above assumptions into (5), one obtains ρ ,

$$\rho(r) = \frac{\rho_0}{\left[c_1 (\rho_0 r^{2(\omega_1+1)})^{m-1} - \frac{\omega_2}{\omega_1+1} \right]^{\frac{1}{m-1}}}, \quad (9)$$

where c_1 is an integration constant. Near the origin ($r \rightarrow 0$), the energy density reaches its maximum and reads

$$\rho(r \rightarrow 0) \sim \frac{\rho_0}{\left(\frac{-\omega_2}{\omega_1+1} \right)^{\frac{1}{m-1}}}, \quad (10)$$

Since $\rho \rightarrow \rho_0$ as $r \rightarrow 0$, therefore, we require that $\omega_2 = -\omega_1 - 1$.

At large r , the energy density behaves as

$$\rho(r \rightarrow \infty) \sim \frac{1}{c_1^{\frac{1}{m-1}} r^{2(\omega_1+1)}}. \quad (11)$$

Now if we assume $m > 0, c_1 > 0$ and $\omega_1 > 0$, the energy density is always positive.

The tangential pressure vanishes in

$$P_t = 0, \quad \rightarrow \quad r = \left(\frac{\rho_0^{-m+1}}{\omega_1 c_1} \right)^{\frac{1}{2(\omega_1+1)(m-1)}}. \quad (12)$$

At this stage, by inserting (9) into the Einstein field equations, one can solve and determine the metric functions. In the following sections, we intend to set precise values for the free parameters, m and ω_1 , to present singularity-free solutions that appear physically, i.e., matchable with compact objects.

III. THE FIRST SOLUTION

An immediate and very relevant case is offered by the choice of the free constant made as:

$$m = \frac{3}{2}, \quad (13a)$$

$$\omega_1 = 2. \quad (13b)$$

Here, we notice that any value given to m and ω_1 leads to a possible solution. However, not all solutions yield a finite value for BH mass. In our choices of constants, we present those values that provide a finite BH mass. Immediately, the tangential pressure, P_t , is given as follows

$$P_t = 2\rho - \frac{3\rho^{\frac{3}{2}}}{\sqrt{\rho_0}} > 0, \quad \rightarrow \quad \begin{cases} 0 < \rho < \frac{4}{9}\rho_0, \\ \left(\frac{1}{2c_1\sqrt{\rho_0}} \right)^{\frac{1}{3}} < r < \infty. \end{cases} \quad (14)$$

The behavior of P_t/ρ_0 in terms of ρ/ρ_0 is shown in Fig. (1). For $\rho = \frac{4}{9}\rho_0$, the tangential pressure vanishes beyond which the strong energy condition (SEC) is violated and the gravitational attraction becomes gravitational repulsion, i.e. for the region near the center $0 \leq r \leq \left(\frac{1}{2c_1\sqrt{\rho_0}} \right)^{\frac{1}{3}}$. For $\frac{1}{9}\rho_0 < \rho < \frac{4}{9}\rho_0$, the dominant energy condition (DEC) is satisfied, i.e., $\rho > P_t$. For $\rho = \frac{16}{81}\rho_0$ or $r = \left(\frac{5}{4}c_1\sqrt{\rho_0} \right)^{\frac{1}{3}}$, the tangential pressure has a maximum value at $P_{t,max} = \frac{32}{243}\rho_0$. For $\frac{4}{81}\rho_0 < \rho < \frac{16}{81}\rho_0$ the sound speed is between $0 \leq v_s = \sqrt{dP/d\rho} \leq 1$. Therefore, the allowed region (shaded region in gray) for which the above conditions are satisfied is: $\frac{1}{9}\rho_0 < \rho < \frac{16}{81}\rho_0$, corresponding to $\left(2/c_1\sqrt{\rho_0} \right)^{\frac{1}{3}} \leq r \leq \left(5/4c_1\sqrt{\rho_0} \right)^{\frac{1}{3}}$. We also display P_t/ρ_0 and ρ/ρ_0 as function of $X = (\pi\rho_0 M^2)^{\frac{1}{3}} r/M$ in the right panel of Fig. (1). We observe that the energy density is regular at the center as expected. Then, it becomes decreasing as r increases. On the other hand, the tangential pressure increases (from negative) with r and vanishes at $X = 0.7211$. This agrees with the condition discussed in (37). The pressure reaches its maximum at $X = 0.9787$.

Furthermore, the metric function is obtained as follows

$$f(r) = 1 - \frac{8\pi\sqrt{\rho_0}}{3c_1 r} + \frac{8\pi\sqrt{\rho_0}}{3c_1 r(1 + c_1\sqrt{\rho_0}r^3)}. \quad (15)$$

To find the physical significance of the parameter c_1 , we consider the behavior of the solution at $r \rightarrow \infty$ as follows

$$f(r) \sim 1 - \frac{8\pi\sqrt{\rho_0}}{3c_1 r} + \frac{8\pi}{3c_1^2 r^4} + \mathcal{O}(r^{-7}) \quad (16)$$

It is easy to figure out that c_1 corresponds to a parameter with dimension $[c_1] = L^{-2}$.

This solution describes the gravitational field of a BH if an outer horizon exists outside the radius of the compact object [61]. To obtain the radius of the object, we focus on its gravitational mass, so having as the total mass of the relativistic gravitating system,

$$M = 4\pi \int_0^\infty r^2 \rho(r) dr = \frac{4\pi\sqrt{\rho_0}}{3c_1}, \quad (17)$$

and assuming that the above mass is equal to $M = \rho_0 R^3$, then we obtain

$$R \sim \left(\frac{M}{\rho_0} \right)^{\frac{1}{3}} \sim \left(\frac{4\pi}{3c_1\sqrt{\rho_0}} \right)^{\frac{1}{3}}. \quad (18)$$

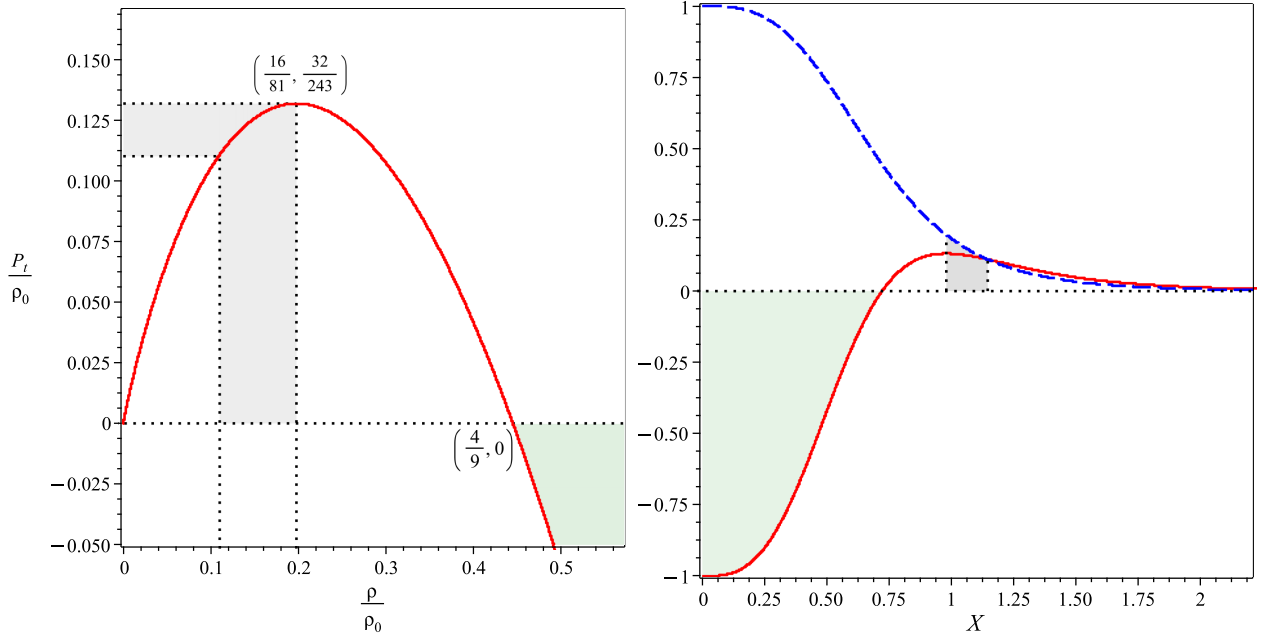


FIG. 1: Left: The behavior of P_t/ρ_0 in terms of ρ/ρ_0 for $m = 3/2$ and $\omega_1 = 2$. Right: The behavior of P_t/ρ_0 (solid line) and ρ/ρ_0 (dash line) in terms of $X = (\pi\rho_0M^2)^{1/3}r/M$. The gray shaded regions are the allowed regions for which $1/9 \leq \rho/\rho_0 \leq 16/81$ (left) and $(15/8)^{1/3} \leq X \leq (3/2)^{1/3}$ (right). In the green-shaded regions, SEC violated.

This can be interpreted as an effective radius if a large mass approximation is assumed.

Nevertheless, the roots of the metric function (15) are

$$r_0 = \frac{\mathcal{A}^{1/3}}{18c_1} + \frac{128\pi^2\rho_0}{9c_1\mathcal{A}^{1/3}} + \frac{8\pi\sqrt{\rho_0}}{9c_1}, \quad (19)$$

$$r_{\pm} = -\frac{\mathcal{A}^{1/3}}{36c_1} - \frac{64\pi^2\rho_0}{9c_1\mathcal{A}^{1/3}} + \frac{8\pi\sqrt{\rho_0}}{9c_1} \pm \frac{i\sqrt{3}}{2} \left(\frac{\mathcal{A}^{1/3}}{18c_1} - \frac{128\pi^2\rho_0}{9c_1\mathcal{A}^{1/3}} \right), \quad (20)$$

where

$$\mathcal{A} = 4096\pi^3\rho_0^{3/2} - \frac{2916c_1^2}{\sqrt{c_1}} + 108c_1\sqrt{\frac{729c_1^2}{\rho_0} - 2048\pi^3}. \quad (21)$$

Depending on the value of the parameters, they can be real or imaginary. The extremal roots, i.e., where they degenerate to one root, are obtained as

$$c_{1,ext} = 9.333\rho_0, \quad (22)$$

$$M_{ext} = \frac{0.44881}{\sqrt{\rho_0}}, \quad \rightarrow \quad r_{ext} = \left(\frac{2}{c_1\sqrt{\rho_0}} \right)^{1/3} = \frac{0.5984134}{\sqrt{\rho_0}}. \quad (23)$$

Thermodynamically, it corresponds to zero temperature and therefore, zero Hawking radiation which is known as BH remnants for an allowed range of parameters [62]. We remark that, for $c_1 > c_{1,ext}$ and $M < M_{ext}$, the horizons disappear.

In Fig. (2), we display the behavior of different radii in terms of c_1M^2 . As it can be seen, for $0 < c_1M^2 < 1.858$, the radius of the object, R , is larger than the outer root of the metric function, r_+ .

This means that, before a certain amount of $c_1M^2 = 1.858$, we have a compact relativistic object, and beyond that, we have a BH solution. Indeed, we have $2M(r_+)/r_+ = 1$ for BHs and for $r > r_+$, we have $2M(R)/R < 1$ [61]. We have also shown this behavior as $4\pi M_{in}/C$ (where C is the circumference of the smallest ring that can engulf the object and M_{in} is the mass within the engulfing sphere.) in terms of c_1M^2 .

For $1.858 < c_1M^2 < 2.018$, we have an object with two horizons with $1.367M < r_{\pm} < 1.613M$ and $R > r_{\pm}$. In this case, we have a compact star with two horizons inside the object. The transition from star to BH happens at $r_{cr} = 1.613M$, $c_{1cr}M^2 = 2.018$. For $c_1 < c_{1ext}$, we have a solution with $r_{\pm} = 0$ and $R \neq 0$, which is known as regular ultra-compact star [63].

In Fig. (2), we also have shown the behavior of the photon sphere radius (gray solid line) versus c_1M^2 . As it can be seen, for $1.522 < c_1M^2 < 1.858$, the photon sphere radius does not vanish and there is a lower bound $c_{1,low}$ for which the photon sphere radius is in the interval $r_{ext} \leq r_{ph} \leq r_{ph}^{sch}$. We denote r_{ph}^{sch} as photon sphere radius of the Schwarzschild black hole.

It is interesting to notice that the behavior of r_i/M versus ρ_0M^2 looks the same, as in Fig. (2), since c_1 and ρ_0 hold the same dimension.

A. Investigating the first solution properties

In the following, we study the metric in (15), in the BH region i.e., $R < r_+$. By expanding the metric function f near the origin, one gets

$$f(r) \sim 1 - \frac{8\pi\rho_0}{3}r^2 + \mathcal{O}(r^5). \quad (24)$$

Accordingly, one can interpret the coefficient of r^2 in the form of a positive effective cosmological constant $\Lambda_{eff} = 8\pi\rho_0$, indicating that the solution near the origin behaves as a de Sitter vacuum. By calculating two curvature invariants the Ricci and the Kretschmann scalars near the origin, we obtain

$$\lim_{r \rightarrow 0} \mathcal{R} = 32\pi\rho_0 = 4\Lambda_{eff}, \quad (25)$$

$$\lim_{r \rightarrow 0} \mathcal{K} = \lim_{r \rightarrow 0} \mathcal{R}_{abcd}\mathcal{R}^{abcd} = \frac{512\pi^2\rho_0^2}{3} = \frac{8}{3}\Lambda_{eff}^2. \quad (26)$$

One can see that, they are finite at $r = 0$, meaning that the first BH solution is free of curvature singularities at the center. However, the curvature invariant does not have a real physical meaning and only provides a tool for a simple and preliminary analysis of spacetime regularity. In physics, we have to look at the geodesic equations and see whether and where they are well defined. Therefore, a basic requirement for regular spacetime should be the completion of all causal geodesics. It is easy to show that a probe particle can reach the point $r = 0$ in a finite amount of proper time. By extension of the geodesics to the negative values, we find that the point $r = \left(\frac{-1}{c_1\sqrt{\rho_0}}\right)^{\frac{1}{3}}$ to be the singularity of metric (15). Therefore, this BH is geodesically incomplete and therefore is not an RBH [64].

In the following, we look for a sign of repulsive gravity. It is known that violation of the strong energy conditions is a signature of repulsive gravity. So, the strong energy condition $\rho + P_r + P_t > 0$, is violated at

$$r_{sec} = \left(\frac{1}{2c_1\sqrt{\rho_0}}\right)^{\frac{1}{3}}. \quad (27)$$

Similarly, the changes in the sign of the Ricci scalar are a signature of topology change of spacetime. Therefore, a computation shows that the Ricci scalar changes its sign at the radius

$$\mathcal{R} = 0 \quad \rightarrow \quad r_R = \left(\frac{2}{c_1\sqrt{\rho_0}}\right)^{\frac{1}{3}}. \quad (28)$$

The eigenvalues of the curvature λ_i according to [65–69], for this metric yields (see Appendix A for details)

$$\begin{aligned} \lambda_1 &= -\frac{8\pi\rho_0(1 + c_1^2\rho_0 r^6 - 7c_1\sqrt{\rho_0}r^3)}{3(1 + c_1\sqrt{\rho_0}r^3)^3}, \\ \lambda_4 &= \frac{8\pi\rho_0}{3(1 + c_1r^3\sqrt{\rho_0})}, \\ \lambda_2 = \lambda_3 = -\lambda_5 = -\lambda_6 &= \frac{4\pi\rho_0(-2 + c_1r^3\sqrt{\rho_0})}{3(1 + c_1r^3\sqrt{\rho_0})^2}. \end{aligned} \quad (29)$$

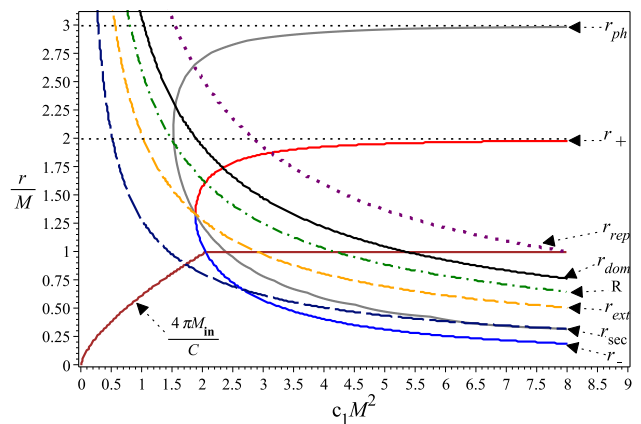


FIG. 2: The radial coordinates of key features in the metric (15) are depicted here: The behavior of r_{\pm}/M , r_{ext}/M , r_{rep}/M , r_{ph}/M and R/M in terms of c_1M^2 for the first BH solution.

From (29), we see that λ_1 and λ_2 change their sign when approaching $r = 0$, indicating the places at which repulsive gravity becomes dominant. The first extremum that is reached when approaching from infinity is located at $r_{rep} = \left(\frac{8+3\sqrt{6}}{2c_1\sqrt{\rho_0}}\right)^{\frac{1}{3}}$, which corresponds to a local minimum of λ_1 . The largest extremum belongs to λ_1 and determines the repulsion radius as r_{rep} , corresponding to the onset of repulsive gravity. Moreover, when approaching the source from infinity, the first zero in λ_1 is at $r_{dom} = \left(\frac{7+3\sqrt{5}}{2c_1\sqrt{\rho_0}}\right)^{\frac{1}{3}}$, which is the point at which repulsive gravity becomes dominant.

In Fig. (2), we compare the behavior of different radii. There, a peculiar point is that the r_{rep}/M curve for $3.097 < c_1M^2$ is smaller than the BH event horizon. For $0 < c_1M^2 < 3.097$, the repulsive gravity appears outside the BHs. Hence, one can wonder whether RBHs and their remnants may be dark energy sources due to their repulsive gravity effects [44].

Another important aspect is the stability of the Cauchy horizon of these BH solutions. In [34, 35] by considering the backreaction between the infalling matter and geometry the stability of Cauchy horizon of black holes has been studied. It has been shown that if the denominator of equation (19) of the paper [35] is nonlinear, then the Cauchy horizon of the black hole is stable under mass inflation. It is easy to show that the denominator is nonlinear for our metric and therefore the Cauchy horizon of this solution is stable.

Here, we investigate the thermodynamical topology of an RBH. As shown in [70, 71], one can introduce the free energy as

$$\mathcal{F} = M - \frac{\mathcal{S}}{\tau} = \frac{r_+}{4} + \frac{\sqrt{9c_1^2r_+^4 + 96\pi}}{12c_1r_+} - \frac{\pi r_+^2}{\tau}, \quad (30)$$

for a BH with mass M , entropy $\mathcal{S} = \pi r_+^2$ and τ can be

thought of as the inverse temperature of a cavity enclosing the BH. One can construct a vector field ϕ as [71]

$$\phi = \left(\frac{\partial \mathcal{F}}{\partial r_+}, -\cot(\theta) \csc(\theta) \right), \quad (31)$$

in which the two parameters r_+ and θ obey $0 < r_+ < \infty$ and $0 \leq \theta \leq \pi$. By solving the equation $\phi^{r_+} = 0$, one can obtain a curve on $r_+ - \tau$ plane. For the first solution, one gets

$$\tau = -\frac{8\pi r_+^3 c_1 \sqrt{9c_1^2 r_+^4 + 96\pi}}{32\pi - c_1 r_+^2 \sqrt{9c_1^2 r_+^4 + 96\pi} - 3c_1^2 r_+^4}. \quad (32)$$

We show the behavior of ϕ^{r_+} in the $r_+ - \tau$ plane in the left figure of Fig. (3). For large $\tau = \tau_1$, there are two intersection points for the BH. The intersection points exactly satisfy the condition $\tau = 1/T$ (where T is the Hawking temperature of a BH) and therefore represent the on-shell BHs. The two intersection points can coincide with each other when $\tau = \tau_c$ and vanish when $\tau < \tau_c$. Therefore, τ_c is an annihilation point which can be found at $\tau_c = 50.40245034r_0/\sqrt{c_1}$ with an arbitrary length scale r_0 set by the size of a cavity surrounding the black hole.

Alternatively, the unit vector field $n = (n^r, n^\theta) = (\phi^{r_+}/|\phi|, \phi^\theta/|\phi|)$, is plotted for $\tau = 65r_0$ in Fig. (3)b, where we find two zero points at $r_+ = 2.324090959r_0, \theta = \pi/2$ and at $r_+ = 4.965244619r_0, \theta = \pi/2$. To determine the winding number of the zero point, we need to construct a closed loop around it and count the changes in the direction of the vector. For this aim, we parametrize the closed loop C_i using the angle s as follows

$$\frac{r_\pm}{r_0} = a \cos(s) + r_c, \quad \theta = b \sin(s) + \frac{\pi}{2} \quad (33)$$

where $0 \leq s \leq 2\pi$ and $(r_c, \pi/2)$ is the center of closed loop. To obtain the change in the direction of the vector, the deflection angle is given by

$$\Omega(s) = \oint_C \epsilon_{ab} n^a n^b \partial_s n^b ds. \quad (34)$$

Then, the winding number is defined as $Q = \Omega(2\pi)/2\pi$.

Using the method described above, we have shown the behavior of deflection angle $\Omega(s)$ for the contours C_1, C_2 and C_3 in Fig (4). From the figure, we clearly see that for C_1 (C_2) with the increases s , Ω increases (decreases) and approaches 2π (-2π) at $s = 2\pi$. Thus, we get $Q_1 = 1$ for C_1 and $Q_2 = -1$ for C_2 as expected. Here we have used $a = 0.6, b = 0.15$. The contour C_3 surrounds the two zero points leading to the winding number $Q_3 = 0$. This is because, as can be seen in Fig (4), Ω firstly decreases, then increases, and finally vanishes at $s = 2\pi$. Here we have used $a = 2.5, b = 0.5$.

Finally, using (17) for the ADM mass and effective cosmological constant $\Lambda_{eff} = 3/L^2 = 8\pi\rho_0$, it is easy to rewrite the metric (15) as follows:

$$f(r) = 1 - \frac{2Mr^2}{r^3 + 2ML^2} \quad (35)$$

which is the Hayward metric considered in [25]. It should be noted that by choosing $m = 3/2$ and $\omega_1 = 1$ the Dymnikova RBH solution is also obtained [15]. Therefore, in this section, we have shown that the Hayward BH can be a solution of Einstein's gravity with an anisotropic perfect fluid with a multi-polytropic equation of state and has a structure like a compact star. But, the remnant of this solution is a regular object with repulsive gravity.

IV. THE SECOND SOLUTION

Here in this section, we consider the second solution which can be obtained by choosing

$$m = \frac{3}{2}, \quad (36a)$$

$$\omega_1 = 3. \quad (36b)$$

Again, the above choice refers to the need for constant BH mass. Particularly, the tangential pressure, P_t , in this case, reads

$$P_t = 3\rho - \frac{4\rho^{\frac{3}{2}}}{\sqrt{\rho_0}} > 0 \rightarrow \begin{cases} 0 < \rho < \frac{9}{16}\rho_0 \\ \left(\frac{1}{3c_1\sqrt{\rho_0}} \right)^{\frac{1}{4}} < r < \infty \end{cases} \quad (37)$$

The behavior of P_t/ρ_0 in terms of ρ/ρ_0 has been shown in Fig. (5). For $0 < \rho < 9\rho_0/16$, the SEC condition is satisfied, and for $\rho = \rho_0/4$ or $r = (1/c_1\sqrt{\rho_0})^{\frac{1}{4}}$, the tangential pressure has a maximum value as $P_{t,max} = \rho_0/4$. For $\rho > 9\rho_0/16$ or $0 < r < (1/(3c_1\sqrt{\rho_0}))^{\frac{1}{4}}$ which is a region close to the center, the SEC is violated. However, the DEC is satisfied when $0 \leq \rho \leq \rho_0/4$. Moreover, for $\rho_0/9 \leq \rho \leq \rho_0/4$, the speed of sound is $0 \leq v_s \leq 1$.

To satisfy all the energy conditions (SEC and DEC) and sound speed limit, we find that the energy density must be restricted to $\rho_0/9 \leq \rho \leq \rho_0/4$ which corresponds to $(1/c_1\sqrt{\rho_0})^{1/4} \leq r \leq (2/(c_1\sqrt{\rho_0}))^{1/4}$. This region is highlighted as a gray area in Fig. (5). We also depict P_t/ρ_0 and ρ/ρ_0 as function of $X = (\pi\rho_0 M^2)^{\frac{1}{3}} r/M$ in the right panel of Fig. (5). We find that the energy density decreases as a function of r . In contrast, the tangential pressure reaches its maximum at $X = \sqrt{2}$ and then vanishes at large r .

In this case, the metric function is obtained as

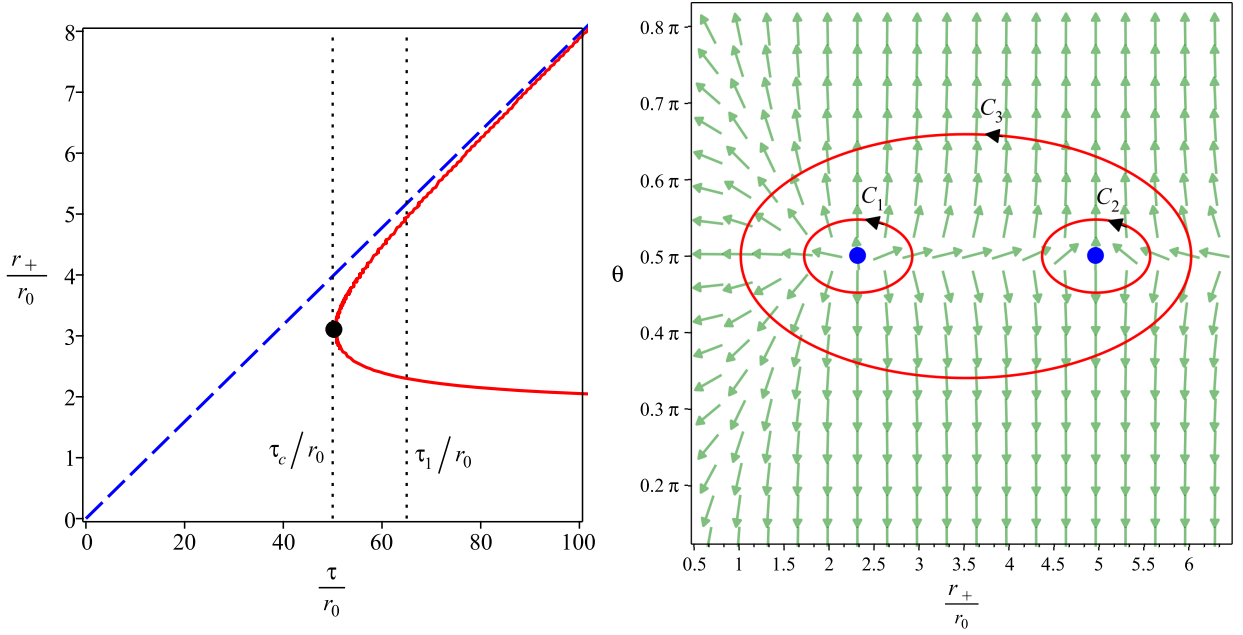


FIG. 3: Left: Zero points of the vector ϕ shown in the $r_+ - \tau$ for $c_1 = 1$. The blue dashed line is for the Schwarzschild BH and the red solid line is for the first solution. The annihilation point for this BH is represented by the black dot with τ_c . There are two RBHs when $\tau = \tau_1$. Right: The red arrows represent the unit vector field n on a the $r_+ - \theta$ plane for $\tau/r_0 = 65$. The zero points are shown with blue dots and the red contours C_i are closed loops surrounding the zero points.

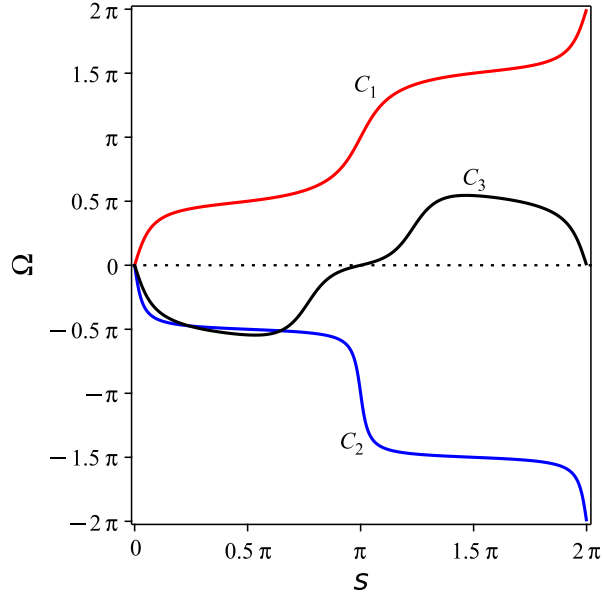


FIG. 4: The deflection angle Ω as a function of s for contours C_i .

$$f(r) = 1 - \frac{2\pi\rho_0 r^2}{1 + c_1\sqrt{\rho_0}r^4} + \frac{\pi\sqrt{2\rho_0}}{2c_1\mathcal{E}^{\frac{1}{4}}r} \left[\ln \left(\frac{r^2 + \sqrt{2}\mathcal{E}^{\frac{1}{4}}r + \sqrt{\mathcal{E}}}{r^2 - \sqrt{2}\mathcal{E}^{\frac{1}{4}}r + \sqrt{\mathcal{E}}} \right)^{\frac{1}{2}} - \arctan \left(\frac{\sqrt{2}r}{\mathcal{E}^{1/4} - \mathcal{E}^{-1/4}r^2} \right) \right], \quad (38)$$

here $\mathcal{E} = (c_1\sqrt{\rho_0})^{-1}$. The asymptotic behavior of the metric function is given

$$f(r) \sim 1 - \frac{\pi^2\sqrt{2}\rho_0^{\frac{5}{8}}}{2c_1^{\frac{3}{4}}r} + \mathcal{O}(r^{-3}), \quad (39)$$

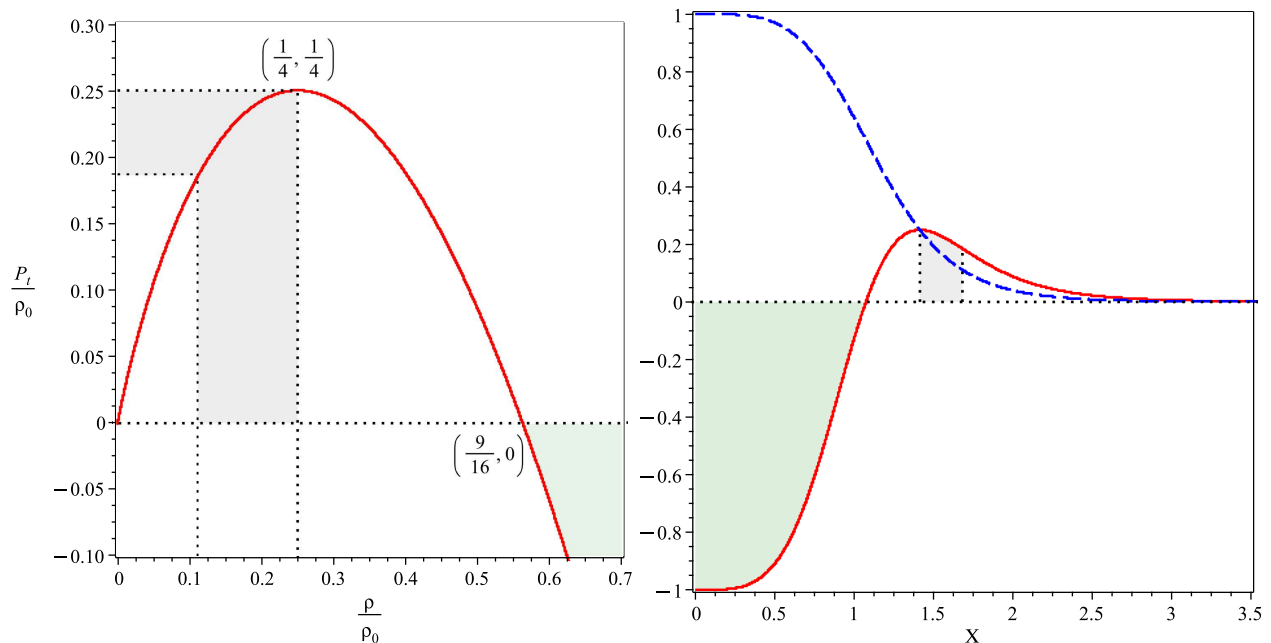


FIG. 5: Left: The behavior of P_t/ρ_0 in terms of ρ/ρ_0 for $m = 3/2$ and $\omega_1 = 3$. Right: The behavior of P_t/ρ_0 (solid line) and ρ/ρ_0 (dash line) in terms of dimensionless quantity $X = (\pi^2 \rho_0 M^2)^{1/3} r/M$. The gray shaded regions are the allowed regions for which $1/9 \leq \rho/\rho_0 \leq 1/4$ (left) and $\sqrt{2} \leq X \leq 2^{3/4}$ (right). In the green-shaded regions, SEC violated.

here, it is easy to show that the dimension of c_1 is $[c_1] = L^{-3}$. The total mass of the system is given by

$$M = 4\pi \int_0^\infty r^2 \rho(r) dr = \frac{\sqrt{2}\pi^2 \rho_0^{5/8}}{4c_1^{3/4}}. \quad (40)$$

Accordingly, the effective radius (R) of the object in the large radius can be approximated as

$$R \sim \left(\frac{M}{\rho_0}\right)^{1/3} = \left(\frac{\sqrt{2}\pi^2}{4c_1^{3/4}\rho_0^{5/8}}\right)^{1/3}. \quad (41)$$

The metric (38) is a BH solution if the largest root of the metric (r_+) is greater than the above radius (R). In Fig. (6), the behavior of different properties of the solution in terms of dimensionless quantity $c_1 M^3$ has been shown. For $0 \leq c_1 M^3 \leq 1.123$, the radius of the object (R) is larger than the larger root of the metric (r_+) (38). and we have also shown this in another language as $4\pi M_{in}/C < 1$ (brown solid curve). This means, in the mentioned range, we have an ultra-compact star. For $c_1 M^3 > 1.123$, since $r_+ > R$, therefore we have a BH solution with $4\pi M_{in}/C = 1$. In the figure, we also have shown the radius of repulsive gravity r_{rep} (dotted line) and dominant repulsive gravity (r_{dom} black solid line).

As can be seen, for $0 \leq c_1 M^3 \leq 1.933$ the radius of repulsive gravity is larger than the radius of an event horizon. Similar to the first solution, this means that the remnant of the BH has a repulsive gravity. In Fig. (6), the behavior of photon sphere radius has been shown in a solid gray line. For the range $0.522 \leq c_1 M^3 \leq 0.849$, the

radius of the photon sphere is not zero $r_{ext} \leq r_{ph} \leq r_{ph}^{sch}$. It should be noted that most of the results in Fig. (6) are obtained numerically. This is because the solution (38) is complicated and finding associated radii cannot be done analytically. Before analysing the near origin behaviour, let us consider the inner horizon of the BH. To check the stability of the Cauchy horizon of the solution under the passing of matter, we shall consider the denominator of the relation (19) of the paper [35]. Since the denominator is nonlinear for our metric, the solution is stable under mass inflation.

The behavior of metric near the origin is given by

$$f(r) \sim 1 - \frac{8\pi\rho_0}{3}r^2 + \mathcal{O}(r^3). \quad (42)$$

Here, one can interpret the coefficient of r^2 as an effective cosmological constant as $\Lambda_{eff} = 8\pi\rho_0$. The behavior of the Ricci and the Kretschmann scalar near the origin is given by

$$\begin{aligned} \lim_{r \rightarrow 0} \mathcal{R} &= 32\pi\rho_0 = 4\Lambda_{eff}, \\ \lim_{r \rightarrow 0} \mathcal{K} &= \frac{512\pi^2\rho_0^2}{3} = \frac{8}{3}\Lambda_{eff}^2. \end{aligned} \quad (43)$$

One can see that they are finite at $r = 0$, meaning that the second BH solution is free of curvature singularities at the center. However, it is easy to show that the space-time metric (38), is also geodesically complete for both massive and massless particles. Since the metric function (38) is continuous across $r = 0$ and the effective potential is finite everywhere, we can extend the metric across

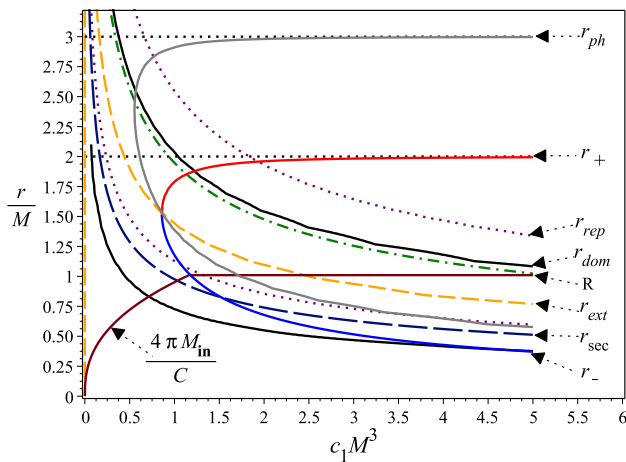


FIG. 6: The radial coordinates of key features in the metric function (38) are depicted here: The behavior of r_{\pm}/M , r_{ext}/M , r_{rep}/M , r_{ph}/M and R/M in terms of c_1M^3 for the second BH solution.

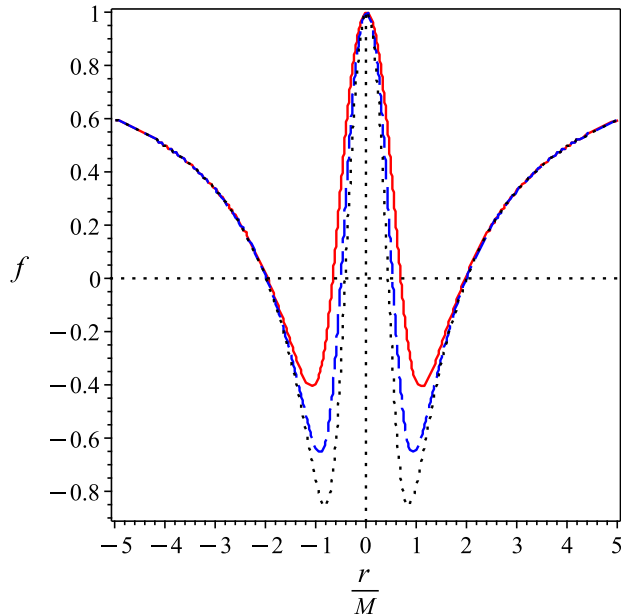


FIG. 7: The behavior of metric function (38) in terms of r/M , for $c_1M^3 = 2, 3, 4$.

$r = 0$ to negative values of r as well (see Fig. 7). Thus a test particle can move from $-\infty$ to $+\infty$ in this space-time, and this takes an infinite amount of proper time. Therefore, this BH is, indeed, regular BH [64].

A. Properties of the second solution

In analogy to the previous section, here we study the thermodynamic topology of RBH. Based on (30) and (31), we can obtain the free energy and components of

the vector field ϕ . Thus, one can plot the corresponding $r_+ - \tau$ diagram, the vector field ϕ , and the deflection angle which are shown in Figs. (8) and (9).

For large $\tau = \tau_1$, there are two intersection points for the BH. The two intersection points coincide with each other when $\tau = \tau_c$ and then vanish when $\tau < \tau_c$. The unit vector field n , is plotted for $\tau = 50r_0$ in Fig. (3)b. We find two zero points at $r_+ = 1.648r_0, \theta = \pi/2$ and at $r_+ = 3.938r_0, \theta = \pi/2$. The winding number of zero points can be determined using (34), after parameterizing the contours using (33). The behavior of deflection angle $\Omega(s)$ for the contours C_1, C_2 and C_3 has been shown in Fig. (9). From the figure, we clearly see that for $C_1(C_2)$ with the increases s , Ω increases (decreases) and approach $2\pi(-2\pi)$ at $s = 2\pi$. Thus, we get $Q_1 = 1$ for C_1 and $Q_2 = -1$ for C_2 as expected. Here we have used $a = 0.6, b = 0.15$. The contour C_3 surrounds the two zero points leading to the winding number $Q_3 = 0$. Because, as can be seen in Fig. (9), by increasing s , Ω firstly decreases and then increases with s . Finally, it vanishes at $s = 2\pi$. Here we have used $a = 2.1, b = 0.5$. As observed, the topological number of this RBH is the same as the previous one, 0, indicating that both belong to the same topological class.

Then, we study the dynamical stability of the BH using the perturbation of the space-time utilizing a real massless scalar field. The evolution of a scalar field in curved spacetime is given by Klein-Gordon equation i.e., $\nabla_\mu \nabla^\mu \Phi = 0$. In a static spherically symmetric background, the scalar field can be assumed to take the following form

$$\Phi = \frac{R(r)}{r} e^{i\omega t} Y(\theta, \phi), \quad (44)$$

where $Y(\theta, \phi)$ is spherical harmonics. The Klein-Gordon equation reads

$$\frac{d^2 R}{dr_*^2} + \left[\omega^2 - f \left(\frac{l(l+1)}{r^2} + \frac{f'}{r} \right) \right] R = 0, \quad (45)$$

where l is orbital quantum number and we have introduced tortoise coordinate $dr_* = dr/f$. The stability of the BH solution is determined via computing quasinormal modes (QNMs). The corresponding boundary condition is that only ingoing scalar wave is allowed at the event horizon and purely outgoing wave at asymptotic infinity. As a result, we obtain a discrete complex eigenfrequency ($\omega = \omega_r + i\omega_i$) or quasinormal frequency.

To obtain quasinormal frequency, we follow Mashhoon's method which offers analytic way to determine ω via the approximation of Pöschl-Teller potential [72]. This method is widely used in obtaining quasinormal frequencies of several spherical symmetric BH spacetimes [72–77]. Additionally, with some alteration, Mashhoon's method is also found to be useful when determining the frequency spectrum of slowly rotating black holes [78, 79].

In Fig. 10, we have given the results related to calculating quasinormal frequencies where the real and imaginary part of the frequencies are plotted against c_1M^3 .

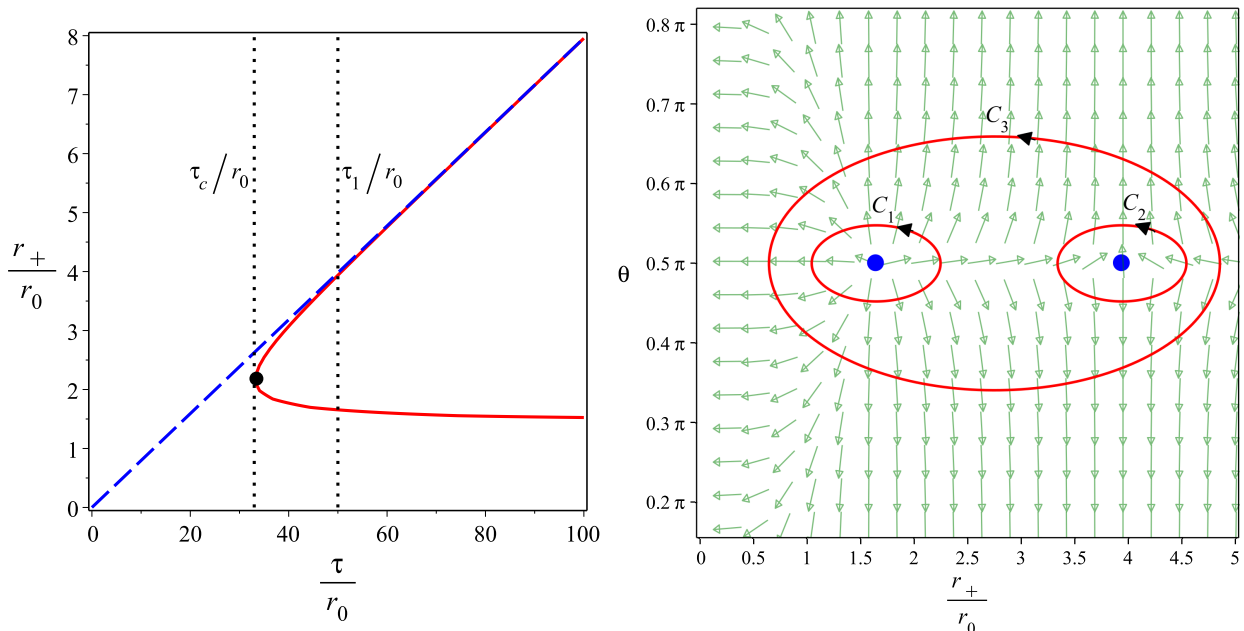


FIG. 8: Left: Zero points of the vector ϕ shown in the $r_+ - \tau$ for $c_1 = 1$. The blue dashed line is for the Schwarzschild BH and the red solid line is for the second solution. The annihilation point for this BH is represented by the black dot with $\tau_c = 33.022$. There are two RBHs when $\tau = \tau_1$. Right: The red arrows represent the unit vector field n on a $r_+ - \theta$ plane for $\tau/r_0 = 50$. The zero points are shown with blue dots and the red contours C_i are closed loops surrounding the zero points.

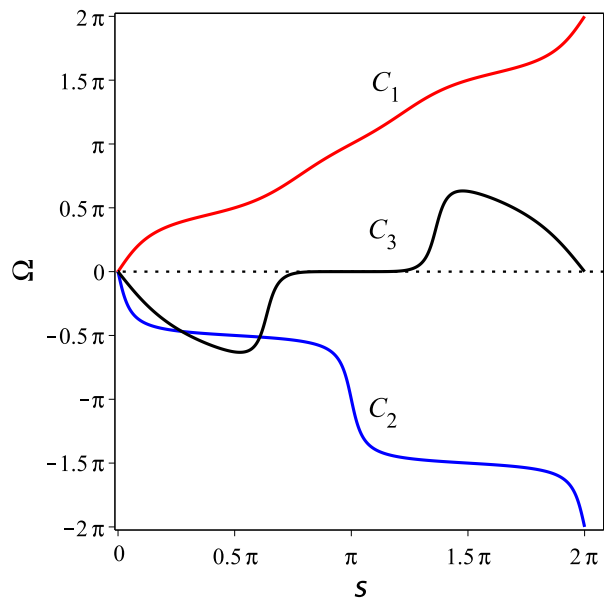


FIG. 9: The deflection angle Ω as a function of s for contours C_i .

The first conclusion that can be drawn from this figure is that the BH remains stable under perturbation. This is because the imaginary part of the frequencies is positive rendering exponential decaying of the perturbation. An additional property is that as l increases, the real part of the frequency increases and the imaginary part

decreases. This means that the wave is less damped as l increases. Also, as it is clear in the figure, with the increase of c_1 , the real part decreases, and the imaginary part increases. This means that c_1 increases the stability of the black hole.

One final remark is, we find that by choosing $m = \omega_1 = 2$, one can obtain a new RBH solution that has almost the same behavior as the solutions presented in this section and it is possible to study it analytically.

V. FINAL OUTLOOKS AND PERSPECTIVES

In this paper, we construct regular black hole solutions in general relativity by assuming anisotropic fluid as a source. Indeed, RBHs have been usually proposed based on purely-phenomenological grounds, for example, lying on theories of non-linear electrodynamics that can generalize the standard Hilbert-Einstein action.

In so doing, we provide a classical strategy to obtain RBHs and start from the widely-used TOV equation, imposing polytropic equations of state.

More precisely, we infer an RBH solution by considering anisotropic perfect fluid as a source with a multipolytropic equation of state. Nevertheless, the structure of the anisotropic pressure consists of radial and transverse components, exhibiting vacuum energy and a multipolytropic counterpart with a linear term plus a power-law contribution.

To do so, we solve the system of equations of motion by setting certain numerical values for the model param-

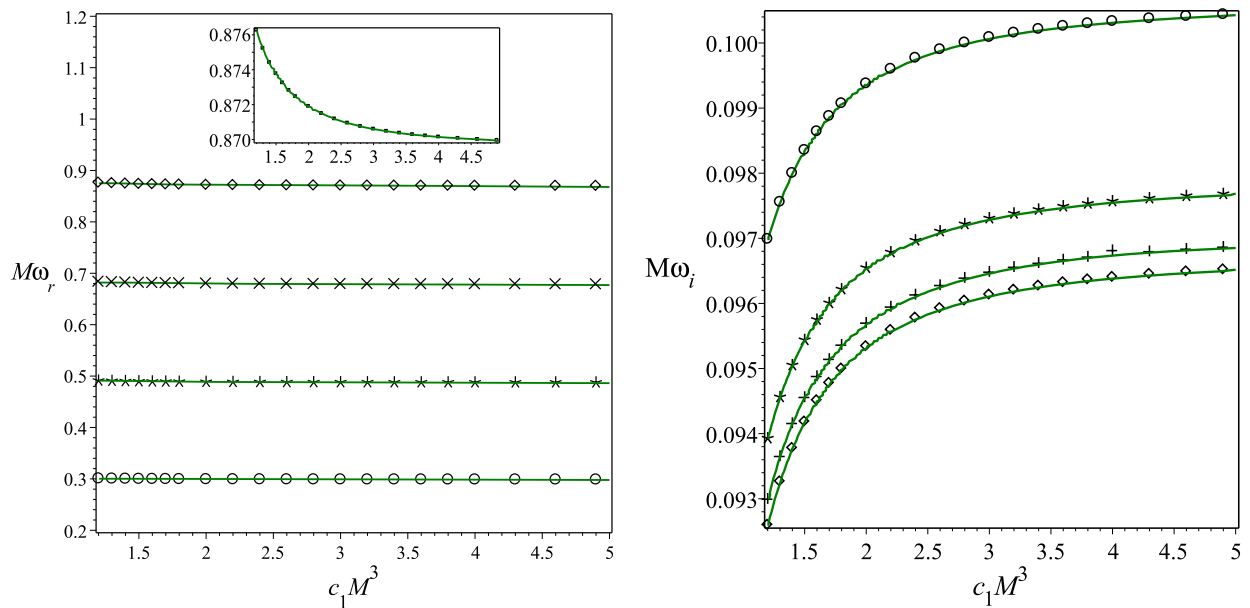


FIG. 10: Left: The real part of the quasinormal frequency for $l = 1, 2, 3, 4$ (bottom to top). Right: The imaginary part of the quasinormal frequency for $l = 1, 2, 3, 4$ (top to bottom).

eters denoted as $m_1, \omega_1, c_1,$ and ρ_0 . These parameters are chosen such that they fulfill physical conditions in order to reproduce viable RBH solutions.

Accordingly, we thus derive two analytical solutions prompting a de Sitter core, i.e., behaving regularly at $r = 0$ and smoothly approaching an asymptotically flat spacetime for large radii. Afterward, we check the regularity of the solutions using curvature scalars and the geodesic completeness of the aforementioned spacetimes.

Interestingly, we seek regions in which gravity switches its sign, within the frameworks of the underlying metrics. Thus, using the eigenvalues of the Riemann curvature tensor, decomposed into its irreducible representation, we consider the effects of repulsive gravity for these metrics to emphasize the peculiarities of the solutions. Moreover, we study the stability of the RBHs under the flow of energy through the inner horizon and, furthermore, we investigate BH thermodynamical stability by counting winding numbers in the thermodynamic parameter space.

We find that these solutions belong to the class of solutions with the topological number $W = 0$. Thus, we conclude that our RBHs can be described by polytropic models similar to other compact objects due to the absence of singularities, suggesting the use of such spacetimes to model physical objects.

As a perspective, we notice that these solutions can be further investigated, for instance, regarding the dynamic stability of these solutions against superradiance scattering and thermodynamics of the BH solutions. In addition, the accretion disk regions [80–82], expected from the aforementioned spacetimes, will be explored. Last but not least, future works can focus on finding out new

metrics, through the same procedure.

Acknowledgements

This research has received funding support from the NSRF via the Program Management Unit for Human Resource and Institutional Development, Research and Innovation grant number *B13F670063*. OL acknowledges financial support from the Fondazione ICSC, Spoke 3 Astrophysics and Cosmos Observations. National Recovery and Resilience Plan (Piano Nazionale di Ripresa e Resilienza, PNRR) Project ID CN_00000013 "Italian Research Center on High-Performance Computing, Big Data and Quantum Computing" funded by MUR Missione 4 Componente 2 Investimento 1.4: Potenziamento strutture di ricerca e creazione di "campioni nazionali di R&S (M4C2-19)" - Next Generation EU (NGEU) GRAB-IT Project, PNRR Cascade Funding Call, Spoke 3, INAF Italian National Institute for Astrophysics, Project code CN00000013, Project Code (CUP): C53C22000350006, cost center STI442016.

Appendix A: Repulsive gravity

In this Appendix, we review the concept of repulsive gravity, used throughout the text and, in particular, its invariant description, in terms of the eigenvalues of the Riemann curvature tensor.

In general, repulsive gravity is certified by investigating the effective potential of any metric, i.e., as the effective potential changes sign, one can infer regions in which the

sign of gravity becomes repulsive. This procedure, albeit physically acceptable, is coordinate-dependent. So, seeking an invariant formalism toward repulsive regions is of utmost importance.

As a naive example, the simplest repulsive solution is offered by a Schwarzschild metric where the gravitational charge has a reversed sign, namely when one assumes the mass to satisfy $M \rightarrow -M$, see [66]. The repulsive sign of gravity cannot be reached as the first-order curvature invariant, the Ricci scalar, vanishes and all the higher-order geometric invariants keep hidden the sign of M , see [65].

Accordingly, to obtain the Riemann curvature tensor in a local orthonormal frame, we choose the orthonormal tetrad e^a as

$$ds^2 = \eta_{ab} e^a \wedge e^b, \quad (\text{A1})$$

with $\eta_{ab} = \text{diag}(-1, 1, 1, 1)$ and $e^a = e_b^a dx^b$. The first and the second Cartan structure equations are

$$\begin{aligned} de^a + \omega_b^a \wedge e^b &= 0, \\ \Omega_b^a &= d\omega_b^a + \omega_c^a \wedge \omega_b^c = \frac{1}{2} R^a_{bcd} e^c \wedge e^d, \end{aligned} \quad (\text{A2})$$

allowing to introduce the connection 1-form ω_b^a and the curvature 2-form Ω_b^a , which determines the tetrad components of the curvature tensor R^a_{bcd} .

Further, to compute the curvature eigenvalues, it is convenient to introduce the convention [83]

$$\begin{aligned} 1 &\rightarrow 01, & 2 &\rightarrow 02, & 3 &\rightarrow 03, & 4 &\rightarrow 23, \\ 5 &\rightarrow 31, & 6 &\rightarrow 12. \end{aligned} \quad (\text{A3})$$

Then, the curvature eigenvalues are easily computed as the eigenvalues of the (6×6) - matrix R_{AB} . Considering

the spacetime geometry (1), after some computations, it is easy to obtain eigenvalues of curvature two form as follows [66]:

$$\begin{aligned} \lambda_1 &= \frac{2hff'' + ff'h' - hf'^2}{4f^2}, \\ \lambda_2 = \lambda_3 &= -\frac{h'}{2r}, \quad \lambda_4 = \frac{1-h}{r^2}, \\ \lambda_5 = \lambda_6 &= \frac{hf'}{2fr}. \end{aligned} \quad (\text{A4})$$

These eigenvalues encapsulate all the information regarding curvature exhibit scalar behavior under coordinate transformations and appear coordinate-independent.

To identify repulsive gravity one adopts the following steps.

- Searching for the sign change of *at least one eigenvalue* that implies the transition from attractive to repulsive gravity. Consequently, the eigenvalue zeros mark the domain where repulsive gravity becomes dominant.
- Finding extremal points in *at least one eigenvalue*, indicating the onset of repulsive effects, as determined by the condition:

$$\frac{\partial \lambda_i}{\partial r} = 0. \quad (\text{A5})$$

The above procedure has been used across the manuscript to identify the repulsive regions and has been widely adopted to cosmological contexts [84] and gravitational solutions [59, 65–67], with promising outcomes indicating that the spacetime alone can exhibit regions where gravity changes its sign.

-
- [1] C. Kiefer, [arXiv:2302.13047 [gr-qc]].
- [2] Kiefer, C., 2012. Quantum Gravity. 3rd ed. Oxford: Oxford University Press.
- [3] W. L. Freedman, Astrophys. J. **919**, no.1, 16 (2021) doi:10.3847/1538-4357/ac0e95 [arXiv:2106.15656 [astro-ph.CO]].
- [4] E. J. Copeland, M. Sami and S. Tsujikawa, Int. J. Mod. Phys. D **15**, 1753-1936 (2006) doi:10.1142/S021827180600942X [arXiv:hep-th/0603057 [hep-th]].
- [5] E. Oks, New Astron. Rev. **93**, 101632 (2021) doi:10.1016/j.newar.2021.101632 [arXiv:2111.00363 [astro-ph.CO]].
- [6] S. Capozziello, P. K. S. Dunsby, O. Luongo, Mon. Not. Roy. Astron. Soc., **509**, 4, 5399–5415, (2021).
- [7] P. K. S. Dunsby, O. Luongo, L. Reverberi, Phys. Rev. D, **94**, 8, 083525, (2016).
- [8] R. Penrose, Phys. Rev. Lett. **14**, 57-59 (1965) doi:10.1103/PhysRevLett.14.57
- [9] R. Penrose, Riv. Nuovo Cim. **1**, 252-276 (1969) doi:10.1023/A:1016578408204
- [10] B. P. Abbott *et al.* [LIGO Scientific and Virgo], Phys. Rev. Lett. **116**, no.6, 061102 (2016) doi:10.1103/PhysRevLett.116.061102 [arXiv:1602.03837 [gr-qc]].
- [11] K. Akiyama *et al.* [Event Horizon Telescope], Astrophys. J. Lett. **875** (2019), L1 doi:10.3847/2041-8213/ab0ec7 [arXiv:1906.11238 [astro-ph.GA]].
- [12] C. Zhang, Y. Ma and J. Yang, Phys. Rev. D **108**, no.10, 104004 (2023) doi:10.1103/PhysRevD.108.104004 [arXiv:2302.02800 [gr-qc]].
- [13] Sakharov, A.D.: Sov. Phys. JETP **22**, 241 (1966)
- [14] Gliner, E.B.: Sov. Phys. JETP **22**, 378 (1966)
- [15] I. Dymnikova, Class. Quant. Grav. **21**, 4417-4429 (2004) doi:10.1088/0264-9381/21/18/009 [arXiv:gr-qc/0407072 [gr-qc]].
- [16] C. Lan, H. Yang, Y. Guo and Y. G. Miao, Int. J. Theor. Phys. **62**, no.9, 202 (2023) doi:10.1007/s10773-023-05454-1 [arXiv:2303.11696 [gr-qc]].
- [17] R. Torres, [arXiv:2208.12713 [gr-qc]].
- [18] Roberto Giambò, Orlando Luongo, Class. Quant. Grav., **41**, 12, 125005, (2024).

- [19] D. Corona, R. Giambò, O. Luongo, *Int. J. Geom. Meth. Mod. Phys.*, **21**, 10, 2440019, (2024).
- [20] Bardeen, J.: Presented at GR5, Tiflis, U.S.S.R., and Published in the Conference Proceedings in the U.S.S.R. (1968)
- [21] E. Ayon-Beato and A. Garcia, *Phys. Rev. Lett.* **80** (1998), 5056-5059 doi:10.1103/PhysRevLett.80.5056 [arXiv:gr-qc/9911046 [gr-qc]].
- [22] I. Dymnikova, *Gen. Rel. Grav.* **24** (1992), 235-242 doi:10.1007/BF00760226
- [23] M. Novello, S. E. Perez Bergliaffa and J. M. Salim, *Class. Quant. Grav.* **17** (2000), 3821-3832 doi:10.1088/0264-9381/17/18/316 [arXiv:gr-qc/0003052 [gr-qc]].
- [24] K. A. Bronnikov, *Phys. Rev. Lett.* **85** (2000), 4641 doi:10.1103/PhysRevLett.85.4641
- [25] S. A. Hayward, *Phys. Rev. Lett.* **96**, 031103 (2006) doi:10.1103/PhysRevLett.96.031103 [arXiv:gr-qc/0506126 [gr-qc]].
- [26] S. N. Sajadi and N. Riazi, *Gen. Rel. Grav.* **49** (2017) no.3, 45 [erratum: *Gen. Rel. Grav.* **52** (2020) no.2, 18] doi:10.1007/s10714-017-2209-8
- [27] A. Kumar, R. K. Walia and S. G. Ghosh, *Universe* **8** (2022) no.4, 232 doi:10.3390/universe8040232 [arXiv:2003.13104 [gr-qc]].
- [28] M. E. Rodrigues, E. L. B. Junior, G. T. Marques and V. T. Zanchin, *Phys. Rev. D* **94** (2016) no.2, 024062 doi:10.1103/PhysRevD.94.024062 [arXiv:1511.00569 [gr-qc]].
- [29] T. Tangphati, M. Youk and S. Ponglertsakul, *JHEAp* **43** (2024), 66-78 doi:10.1016/j.jheap.2024.06.009 [arXiv:2312.16614 [gr-qc]].
- [30] Wilson, Alan Herries. "A Generalised Spheroidal Wave Equation." Proceedings of The Royal Society A: Mathematical, Physical and Engineering Sciences 118 (1928): 617-635.
- [31] P. Bueno, P. A. Cano and R. A. Hennigar, [arXiv:2403.04827 [gr-qc]].
- [32] M. S. Ma and R. Zhao, *Class. Quant. Grav.* **31**, 245014 (2014) doi:10.1088/0264-9381/31/24/245014 [arXiv:1411.0833 [gr-qc]].
- [33] L. Balart and S. Fernando, *Mod. Phys. Lett. A* **32**, no.39, 1750219 (2017) doi:10.1142/S0217732317502194 [arXiv:1710.07751 [gr-qc]].
- [34] R. Carballo-Rubio, F. Di Filippo, S. Liberati, C. Pacilio and M. Visser, *JHEP* **09**, 118 (2022) doi:10.1007/JHEP09(2022)118 [arXiv:2205.13556 [gr-qc]].
- [35] A. Bonanno, A. P. Khosravi and F. Saueressig, *Phys. Rev. D* **103**, no.12, 124027 (2021) doi:10.1103/PhysRevD.103.124027 [arXiv:2010.04226 [gr-qc]].
- [36] Z. Li and C. Bambi, *JCAP* **01**, 041 (2014) doi:10.1088/1475-7516/2014/01/041 [arXiv:1309.1606 [gr-qc]].
- [37] I. Dymnikova and K. Kraav, *Universe* **5**, no.7, 163 (2019) doi:10.3390/universe5070163
- [38] Y. Ling and M. H. Wu, *Symmetry* **14**, no.11, 2415 (2022) doi:10.3390/sym14112415 [arXiv:2205.08919 [gr-qc]].
- [39] S. H. Hendi, S. N. Sajadi and M. Khademi, *Phys. Rev. D* **103**, no.6, 064016 (2021) doi:10.1103/PhysRevD.103.064016 [arXiv:2006.11575 [gr-qc]].
- [40] A. Flachi and J. P. S. Lemos, *Phys. Rev. D* **87**, no.2, 024034 (2013) doi:10.1103/PhysRevD.87.024034 [arXiv:1211.6212 [gr-qc]].
- [41] X. C. Cai and Y. G. Miao, *Phys. Rev. D* **102**, no.8, 084061 (2020) doi:10.1103/PhysRevD.102.084061 [arXiv:2008.04576 [gr-qc]].
- [42] S. N. Sajadi, N. Riazi and S. H. Hendi, *Eur. Phys. J. C* **79**, no.9, 775 (2019) doi:10.1140/epjc/s10052-019-7272-8 [arXiv:2003.13472 [gr-qc]].
- [43] H. Yang and Y. G. Miao, *Chin. Phys. C* **47**, no.7, 075101 (2023) doi:10.1088/1674-1137/acdc7 [arXiv:2211.15130 [gr-qc]].
- [44] M. Calzà, D. Pedrotti and S. Vagnozzi, *Phys. Rev. D* **111**, no.2, 024009 (2025) doi:10.1103/PhysRevD.111.024009 [arXiv:2409.02804 [gr-qc]].
- [45] F. Shojai, A. Sadeghi and R. Hassannejad, *Class. Quant. Grav.* **39**, no.8, 085003 (2022) doi:10.1088/1361-6382/ac5924 [arXiv:2202.14024 [gr-qc]].
- [46] V. V. Kiselev, *Class. Quant. Grav.* **20** (2003), 1187-1198 doi:10.1088/0264-9381/20/6/310 [arXiv:gr-qc/0210040 [gr-qc]].
- [47] L. C. N. Santos, *Eur. Phys. J. C* **84** (2024) no.12, 1318 doi:10.1140/epjc/s10052-024-13664-y [arXiv:2411.18804 [gr-qc]].
- [48] M. Chaisi and S. D. Maharaj, *Pramana* **66**, 609-614 (2006) doi:10.1007/BF02704504 [arXiv:gr-qc/0602030 [gr-qc]].
- [49] K. Dev and M. Gleiser, *Gen. Rel. Grav.* **34**, 1793-1818 (2002) doi:10.1023/A:1020707906543 [arXiv:astro-ph/0012265 [astro-ph]].
- [50] K. Dev and M. Gleiser, *Gen. Rel. Grav.* **35**, 1435-1457 (2003) doi:10.1023/A:1024534702166 [arXiv:gr-qc/0303077 [gr-qc]].
- [51] B. V. Ivanov, *Phys. Rev. D* **65**, 104001 (2002) doi:10.1103/PhysRevD.65.104001 [arXiv:gr-qc/0203070 [gr-qc]].
- [52] T. Harko and M. K. Mak, *Chin. J. Astron. Astrophys.* **2**, no.3, 248 (2002) doi:10.1088/1009-9271/2/3/248
- [53] M. K. Mak and T. Harko, *Proc. Roy. Soc. Lond. A* **459**, 393-408 (2003) doi:10.1098/rspa.2002.1014 [arXiv:gr-qc/0110103 [gr-qc]].
- [54] T. Ortin, Cambridge University Press, 2015, ISBN 978-0-521-76813-9, 978-0-521-76813-9, 978-1-316-23579-9 doi:10.1017/CBO9781139019750
- [55] R.C. Tolman. "Relativity, Thermodynamics and Cosmology". Oxford University Press, (1934).
- [56] J.R. Oppenheimer and G.M. Volkoff. *Physical Review*, 55(4): 374381 (1939).
- [57] S. N. Sajadi and N. Riazi, *Can. J. Phys.* **98**, no.11, 1046-1054 (2020) doi:10.1139/cjp-2019-0524 [arXiv:1611.04343 [gr-qc]].
- [58] N. Riazi, S. S. Hashemi, S. N. Sajadi and S. Assyae, *Can. J. Phys.* **94**, no.10, 1093-1101 (2016) doi:10.1139/cjp-2016-0365 [arXiv:1507.03420 [gr-qc]].
- [59] S. N. Sajadi, M. Khodadi, O. Luongo and H. Quevedo, *Phys. Dark Univ.* **45**, 101525 (2024) doi:10.1016/j.dark.2024.101525 [arXiv:2312.16081 [gr-qc]].
- [60] D.D. Clayton. "Principles of Stellar Evolution and Nucleosynthesis". McGraw-Hill, (1968).
- [61] G. Liu and Y. Peng, *Nucl. Phys. B* **970**, 115485 (2021) doi:10.1016/j.nuclphysb.2021.115485
- [62] A. H. Chamseddine, V. Mukhanov and T. B. Russ, *JHEP* **10**, 104 (2019) doi:10.1007/JHEP10(2019)104 [arXiv:1908.03498 [hep-th]].
- [63] S. H. Völkel and K. D. Kokkotas, *Class. Quant. Grav.*

- 34**, no.17, 175015 (2017) doi:10.1088/1361-6382/aa82de [[arXiv:1704.07517](#) [gr-qc]].
- [64] T. Zhou and L. Modesto, Phys. Rev. D **107**, no.4, 044016 (2023) doi:10.1103/PhysRevD.107.044016 [[arXiv:2208.02557](#) [gr-qc]].
- [65] O. Luongo and H. Quevedo, Class. Quant. Grav. **41**, no.12, 125011 (2024) doi:10.1088/1361-6382/ad4ae4 [[arXiv:2305.11185](#) [gr-qc]].
- [66] O. Luongo and H. Quevedo, Phys. Rev. D **90**, no.8, 084032 (2014) doi:10.1103/PhysRevD.90.084032 [[arXiv:1407.1530](#) [gr-qc]].
- [67] O. Luongo, H. Quevedo and S. N. Sajadi, Gen. Rel. Grav. **56**, no.2, 17 (2024) doi:10.1007/s10714-024-03207-x [[arXiv:2311.13264](#) [gr-qc]].
- [68] R. Giambò, O. Luongo, H. Quevedo, Phys. Dark Univ., **30**, 100721, (2020).
- [69] O. Luongo, H. Quevedo, *Toward an invariant definition of repulsive gravity*, MG 12, 1029-1031, ArXiv: 1005.4532, (2010).
- [70] S. W. Wei, Y. X. Liu and R. B. Mann, Phys. Rev. Lett. **129**, no.19, 191101 (2022) doi:10.1103/PhysRevLett.129.191101 [[arXiv:2208.01932](#) [gr-qc]].
- [71] S. W. Wei and Y. X. Liu, Phys. Rev. D **105**, no.10, 104003 (2022) doi:10.1103/PhysRevD.105.104003 [[arXiv:2112.01706](#) [gr-qc]].
- [72] V. Ferrari and B. Mashhoon, Phys. Rev. D **30**, 295 (1984).
- [73] V. Cardoso and J. P. S. Lemos, Phys. Rev. D **67** (2003), 084020 doi:10.1103/PhysRevD.67.084020 [[arXiv:gr-qc/0301078](#) [gr-qc]].
- [74] C. Molina, Phys. Rev. D **68** (2003), 064007 doi:10.1103/PhysRevD.68.064007 [[arXiv:gr-qc/0304053](#) [gr-qc]].
- [75] S. Ponglertsakul, P. Burikham and L. Tannukij, Eur. Phys. J. C **78** (2018) no.7, 584 doi:10.1140/epjc/s10052-018-6057-9 [[arXiv:1803.09078](#) [gr-qc]].
- [76] P. Burikham, S. Ponglertsakul and T. Wuthicharn, Eur. Phys. J. C **80** (2020) no.10, 954 doi:10.1140/epjc/s10052-020-08528-0 [[arXiv:2010.05879](#) [gr-qc]].
- [77] T. Wuthicharn, S. Ponglertsakul and P. Burikham, Int. J. Mod. Phys. D **31** (2022) no.01, 2150127 doi:10.1142/S0218271821501273 [[arXiv:1911.11448](#) [gr-qc]].
- [78] V. Ferrari and B. Mashhoon, Phys. Rev. Lett. **52** (1984) no.16, 1361 doi:10.1103/PhysRevLett.52.1361
- [79] S. Ponglertsakul and B. Gwak, Eur. Phys. J. C **80** (2020) no.11, 1023 doi:10.1140/epjc/s10052-020-08616-1 [[arXiv:2007.16108](#) [gr-qc]].
- [80] K. Boshkayev, A. Idrissov, O. Luongo, D. Malafarina, Mon. Not. Roy. Astron. Soc., **496**, 2, 1115-1123, (2020).
- [81] K. Boshkayev, T. Konysbayev, E. Kurmanov, O. Luongo, D. Malafarina, *et al.*, Phys. Rev. D, **104**, 8, 084009, (2021).
- [82] E. Kurmanov, K. Boshkayev, R. Giambò, T. Konysbayev, O. Luongo, *et al.*, Astrophys. J., **925**, 2, 210, (2022).
- [83] C. W. Misner, K. S. Thorne, and J. A. Wheeler, Gravitation (W. H. Freeman, San Francisco, 1973), ISBN 978-0-7167-0344-0, 978-0-691-17779-3.
- [84] O. Luongo and H. Quevedo, Found. Phys. **48**, no.1, 17-26 (2018) doi:10.1007/s10701-017-0125-0 [[arXiv:1507.06446](#) [gr-qc]].